8-2020

# The Structure and Symmetry of the Radial Spoke Protein Complex in *Chlamydomonas* Flagella

Emiliya Poghosyan

Ioan Iacovache

Lenka Faltova

Alexander Leitner

Pinfen Yang

*See next page for additional authors*

## Authors

Emiliya Poghosyan, Ioan Iacovache, Lenka Faltova, Alexander Leitner, Pinfen Yang, Dennis R. Diener, Ruedi Aebersold, Benoit Zuber, and Takashi Ishikawa

© 2020. Published by The Company of Biologists Ltd | Journal of Cell Science (2020) 133, jcs245233. doi:10.1242/jcs.245233

RESEARCH ARTICLE

# The structure and symmetry of the radial spoke protein complex in *Chlamydomonas* flagella

**Emiliya Poghosyan[1,2], Ioan Iacovache[3], Lenka Faltova[1], Alexander Leitner[4], Pinfen Yang[5], Dennis R. Diener[1], Ruedi Aebersold[4,6], Benoit Zuber[3] and Takashi Ishikawa[1,2,*]**

## ABSTRACT

The radial spoke is a key element in a transducer apparatus controlling the motility of eukaryotic cilia. The transduction biomechanics is a long-standing question in cilia biology. The radial spoke has three regions – a spoke head, a bifurcated neck and a stalk. Although the neck and the stalk are asymmetric, twofold symmetry of the head has remained controversial. In this work we used single particle cryo-electron microscopy (cryo-EM) analysis to generate a 3D structure of the whole radial spoke at unprecedented resolution. We show the head region at 15 Å (1.5 nm) resolution and confirm twofold symmetry. Using distance constraints generated by cross-linking mass spectrometry, we locate two components, RSP2 and RSP4, at the head and neck regions. Our biophysical analysis of isolated RSP4, RSP9, and RSP10 affirmed their oligomeric state. Our results enable us to redefine the boundaries of the regions and propose a model of organization of the radial spoke component proteins.

**KEY WORDS: Cilia, Cryo-electron microscopy, Dynein, Flagella, Microtubule, Radial spoke, Cross-link mass spectrometry**

## INTRODUCTION

Motile cilia and flagella are ubiquitous organelles present in many eukaryotic cells and are important for diverse cellular functions. The core axonemal ultrastructure of motile cilia and flagella is composed of a characteristic '9 microtubule doublets+2 central pair' arrangement. The entire structure consists of inner and outer dyneins as well as several different regulators of ciliary motion, such as radial spokes. The radial spoke (RS) complex protrudes from the A-tubule of microtubule doublets towards the central pair apparatus in a characteristic 'T'-shape structure. The RS complex appears in pairs or triplets depending on the species. In *Chlamydomonas reinhardtii*, the species used in this study, there are two spokes, RS1 and RS2, and a small protrusion that corresponds to RS3 in other organisms (Pigino et al., 2011; Barber et al., 2012). RS1 and RS2 consist of a head region composed of radial spoke proteins RSP1, -4, -6, -9 and -10; a bifurcated neck region with RSP2, -23 and -16; and a stalk region with RSP3, -5, -7, -8, RSP11–RSP15 and RSP17–RSP22 (Yang et al., 2006).

The radial spoke protein complex in *C. reinhardtii* flagella has been the subject of studies for more than forty years. Among those are pioneering works of spoke complex purification (Yang et al., 2006; Kelekar et al., 2009), identification of the individual radial spoke proteins (Piperno et al., 1981; Yang et al., 2001, 2006; Patel-King et al., 2004) as well as the low-resolution structural comparison between different species (Pigino et al., 2011, 2012; Barber et al., 2012). Nonetheless, important discrepancies remain in the field, which could be resolved with better structural information of the complex. Prominent among these discrepancies is the pseudo-twofold symmetry of the head region of the spoke complex, which was first shown from an intermediate-resolution (~30 Å, ~3 nm) structure of a 96 nm repeating unit (Pigino et al., 2011; Barber et al., 2012). Later, this notion was questioned in the work from Oda and colleagues, who proposed a model where the head region is asymmetric (Oda et al., 2014). This model was derived from a cryo-electron tomography structure with a 9-kDa biotin carboxyl carrier protein (BCCP)-tagged RSP4 and RSP6. Yet another discrepancy in the field is in exact stoichiometry and interactions of the proteins residing in the head and neck subunits of the RS complex. One example is the positioning of RSP4 within the spoke head, which according to glutathione-S-transferase (GST) pull-down assays of recombinantly expressed head and neck RSPs (Kohno et al., 2011) is located as a pivot interacting with RSP1, -9 and -10 and, in contrast, is localized at the periphery of the RS head complex according to more recent structural studies conducted by Oda and colleagues using tagged RSP4. Therefore, the important goals of this study were to understand the molecular architecture and protein–protein interactions in the spoke head and neck regions of the complex as well as to validate or refute pseudo-twofold symmetry of the spoke head.

To examine symmetry of the RS head and characterize protein architecture at the spoke head and neck regions, we conducted single particle cryo-electron microscopy (cryo-EM) analysis. We could not obtain enough purity and yield of the radial spoke using the classical protocol (Kelekar et al., 2009). Therefore we developed and optimized a protocol for RS complex isolation for single particle cryo-EM studies. By combining the results from isolated RS complex with sub-tomogram averaging of flagella we could orient the RS structure in the context of the whole cilia. Single particle analysis results from an isolated RS complex yielded, for the first time, 15 Å (1.5 nm) resolution of the head region (Fig. S2). It validates the pseudo twofold symmetry in the head region of the complex, which is not present in the stalk. In addition, in order to fill a gap between our intermediate resolution structural map and complementary biochemical information, we have employed cross-linking mass spectrometry, used to identify protein–protein interfaces at amino acid resolution (Leitner et al., 2016). Cross-linking mass spectrometry of the RS complex isolated by the method described

[1]Paul Scherrer Institute, Department of Biology and Chemistry, Forschungsstrasse 111, 5232 Villigen PSI, Switzerland. [2]ETH Zurich, Department of Biology, Wolfgang-Pauli-Strasse 27, 8093 Zürich, Switzerland. [3]University of Bern, Institute of Anatomy, Baltzerstrasse 2, 3012 Bern, Switzerland. [4]ETH Zurich, Department of Biology, Institute of Molecular Systems Biology, Otto-Stern-Weg 3, 8093 Zürich, Switzerland. [5]Department of Biological Sciences, Marquette University, Milwaukee, WI 53233, USA. [6]University of Zurich, Faculty of Science, Rämistrasse 71, 8006 Zürich, Switzerland.

*Author for correspondence (takashi.ishikawa@psi.ch)

A.L., 0000-0003-4126-0725; R.A., 0000-0002-9576-3267; B.Z., 0000-0001-7725-5579; T.I., 0000-0002-1976-7477

**Handling Editor: David Stephens**
**Received 14 February 2020; Accepted 25 June 2020**

Journal of Cell Science (2020) 133, jcs245233. doi:10.1242/jcs.245233

here allowed us to localize the RSP2 and RSP4 subunits in our structure and, combined with previously published results from flagella cross-linking and GST pull-down assays, to suggest the localization of the head proteins RSP6, RSP9, RSP10 and RSP1 as well as another neck protein, RSP23 for which the localization was previously unknown. With our proposed protein organization in the RS head and neck units we have been able to explain the discrepancy between estimations from the structure and biochemical data for protein–protein interactions, thus providing a model of protein arrangement that summarizes the research done so far.

## RESULTS

### Improved RS purification from *Chlamydomonas* flagella for single particle cryo-EM

In this work we developed a new RS purification protocol. Purification based on the original protocols (Kelekar et al., 2009; Yang et al., 2006), which use sucrose density gradient centrifugation, did not provide samples of sufficient quality for cryo-electron microscopy. They contained substantial amounts of contaminants of tubulin as well as small particles and aggregates, which are probably disassembled or denatured RS proteins (see transmission electron micrographs in Fig. 1A). Furthermore, the unexpectedly low yield of intact RS complexes (Fig. 1A; <1 mg/ml for cryo-grid preparation from an initial cell culture volume of 6×4 L) might be explained by progressive deterioration of the intact RS during the long gradient centrifugation protocol. To overcome these issues and shorten purification time we used a transgenic *Chlamydomonas* strain expressing 12×His-tagged RSP3 for affinity purification of the spoke complex. The improved yield afforded by this protocol allowed scaling down the initial culture volume to 2×4 L and thus accelerated the purification procedure. It also resulted in decreased aggregation of radial spokes (Fig. 1B). Although some RS proteins were still lost in the flow-through during affinity purification, and the final eluate still contained some tubulin (black arrow on the SDS–PAGE gel in Fig. 1B), >90% of the particles in the eluate could be recognized as RS, as shown by negative-stain transmission electron microscopy (TEM) in Fig. 1B.

### 3D structure of RS and its twofold symmetry at the head region

In order to address the question of molecular interactions of the spoke head and neck regions along with the presence of pseudo-twofold symmetry at the spoke head, we aimed to obtain high-resolution structural details from the RS head and neck regions, as compared to

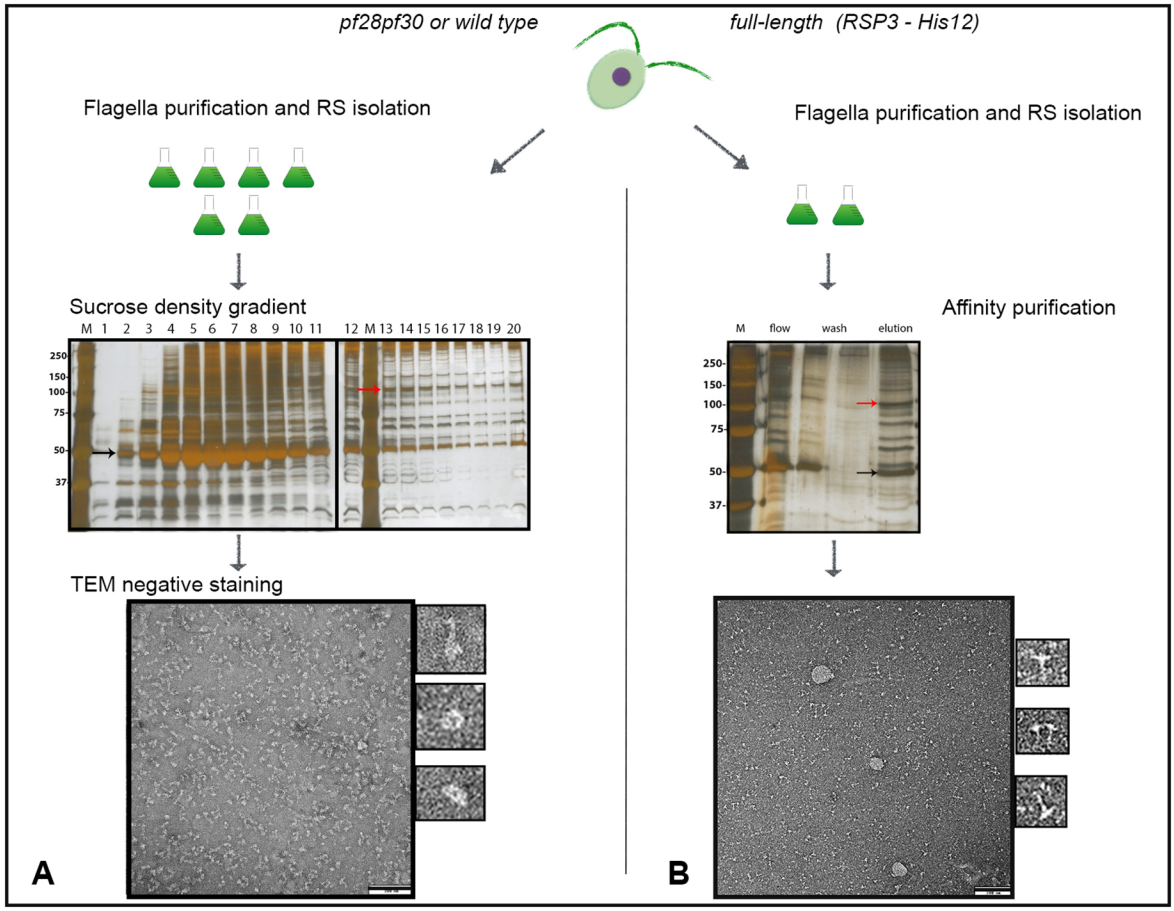


**Fig. 1. Purification of the RS complex.** (A) Using previously established protocols (see Materials and Methods) that require a relatively large initial cell culture volume (6×4 L) and lengthy (~13–14 h) sucrose density gradient centrifugation resulted in RS-enriched fractions (red arrow, RSP1 and RSP2) with considerable tubulin contamination (black arrow) apparent from the silver-stained SDS–PAGE gel. Below is a TEM negative stained micrograph with side panels showing a 4×-magnified gallery of particles where only one out of three particles showed the characteristic 'T' shape of the RS complex. (B) In contrast, the procedure optimized in this work simplified the purification by using a 12×His-tagged full-length RSP3 transgenic strain. The one-step affinity purification procedure resulted in less contaminated, intact spoke complexes, as seen from the silver-stained SDS–PAGE gel and in negative stained micrographs. Red arrow, RSP1 and RSP2; black arrow, tubulin; M, molecular weight markers (kDa). Scale bars: 200 nm.

Journal of Cell Science (2020) 133, jcs245233. doi:10.1242/jcs.245233

all the previous reports (~30 Å, ~3 nm). We thus applied single particle cryo-EM analysis to the affinity-purified RS specimen.

Compared with cryo-electron tomography followed by sub-tomogram averaging of wild-type axonemes from *C. reinhardtii* (Fig. 2A,D), primary features in this structure, such as peripheral protrusions of the head plate (Fig. 2A,B, blue circle), a bifurcated neck region (yellow arrows in Fig. 2D,E) as well as characteristic protrusion in the stalk region of the spoke (blue circle in Fig. 2D,E), were validated. In addition, differences in details between the structure from sub-tomogram averaging and single particle analysis in the head (Fig. 2C, blue circles), neck (Fig. 2E,F, yellow circles) and stalk regions (Fig. 2E, blue circle) were observed.

Both methods demonstrate twofold symmetry at the spoke head region (Fig. 2A,B), whereas the neck and stalk regions do not show symmetry. Based on this result, we further analyzed the structure of the spoke head by masking the head region and imposing twofold symmetry. This allowed us to reconstruct the head region at 15 Å (1.5 nm) resolution (Fig. S2) and revealed further details (Fig. 2C). The structure with twofold symmetry clearly shows spike-like protrusions (yellow arrows in Fig. 2C). Importantly these protrusions were vaguely visible already in the 2D class averages from an unsymmetrized dataset (Fig. S3). The obtained resolution was ~20 Å (~2 nm). By masking the head region, we could improve resolution up to 15 Å (1.5 nm), indicating high flexibility at the stalk region. Because of this, we could not highlight differences between RS1 and RS2, since their major difference is located at the base of the RS stalk. The still limited resolution of the RS head suggested flexibility within the RS head. To sort heterogeneity and improve resolution would require a much larger scale of data acquisition as compared to the current study.

### Cross-linking mass spectrometry and assignment of RSP2 and RSP4 in the cryo-EM map

To further identify protein–protein interactions within the RS complex, we performed on-bead cross-linking experiments with the immobilized, affinity-tagged complex bound to $Co^{2+}$ beads. We used the amine-reactive reagent disuccinimidyl suberate (DSS) (Herzog et al., 2012) with a spacer length of 11.4 Å (1.14 nm) that predominantly links lysine side chains. Despite limitations in sample amount and purity, we were able to identify a cross-link between RSP2, an RS neck protein, and RSP4, a RS head protein, in two independent experiments with two different concentrations of DSS. In particular, the loop downstream from the N-terminal Dpy-30 dimerization/docking domain in RSP2 was determined to be in close spatial proximity to the N-terminal region of RSP4 (Fig. 3A). The unique narrow interface between the neck and the head regions in one symmetrical unit of our density map is the most likely position of their binding site (see Fig. 3B,C). The rest of RSP4 likely makes up the protrusion extending from this juncture (green in Fig. 3B). The difference map between BCCP-tagged (N-terminal tag) RSP4 and

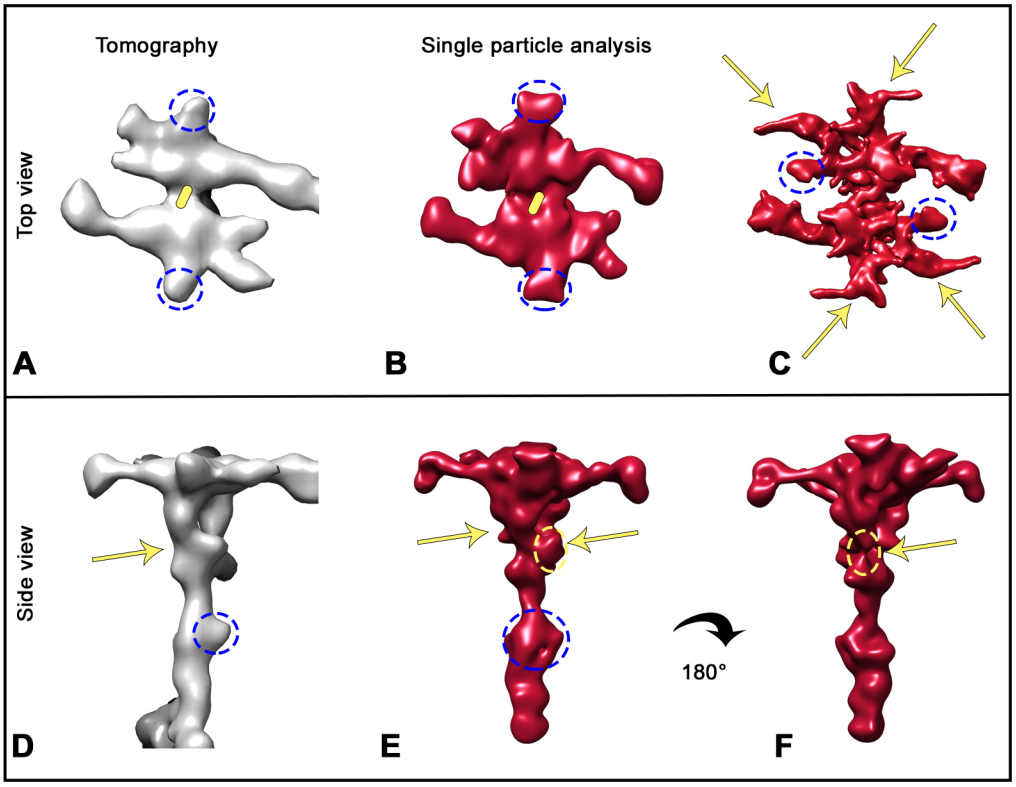


**Fig. 2. Structural comparison of the RS complex using electron cryo-tomography and single particle cryo-electron microscopy.** Our tomographic reconstruction (A,D) together with the structure from single particle analysis (B,E) confirmed pseudo twofold symmetry of the spoke head with an axis perpendicular to the figure plane indicated by yellow ellipse (see A,B). The left side of the structures in A and D correspond to the direction of the minus end of microtubule doublets. The symmetry is broken further down at the intersection between the spoke neck and stalk units (E,F), where differences at both ends (E,F; 180° rotation angle along the stalk axis) of the bifurcated neck are marked with a yellow ellipse and indicated by arrows. Our refinement based on twofold symmetry of the head region of the complex (C) resulted in more detailed structure with additional fine details at the periphery of the spoke complex (yellow arrows, C), which were not seen before. Blue dashed circles indicate identical regions in A,B, and D,E, where differences in details between structures from sub-tomogram averaging and single particle analysis can be observed. Areas in blue circles in C indicate structure detected by symmetrization.

Journal of Cell Science (2020) 133, jcs245233. doi:10.1242/jcs.245233

| Cross-linked protein | Cross-linked region | Predicted motif |
|---|---|---|
| RSP2 | YVKNAEVEGNFYR[59] | DPY-30 |
| RSP4 | [56]KSTFDPK | None |

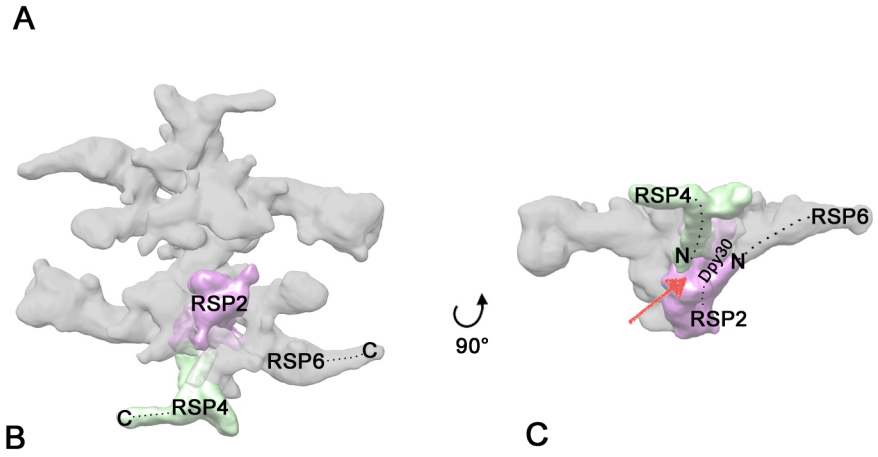


**Fig. 3. Interactions between RSP2 and RSP4 confirmed and localized using cross-linking mass spectrometry.** (A) The cross-linked peptides are near the amino terminus of RSP2 (YVKNAEVEGNFYR[59]; at its Dpy-30 domain for dimerization and docking) and RSP4 ([56]KSTFDPK). (B,C) The amino and carboxy termini of RSP4 and RSP6 are indicated in our single particle structure, based on Oda et al. (2014) The volume presumed to enclose RSP4 is colored green and RSP2 is colored magenta.

untagged wild-type (WT) RSP4 (Oda et al., 2014) supports this assignment. The likely position of the C terminus of RSP4 in their difference map (EMD-5849) is exactly at the tip of this protrusion in our map (Fig. S1). The volume of this protrusion closely matches the volume expected for one monomer of RSP4, as computed from its sequence (56 $nm^3$) (Table S1). Comparison with difference maps between BCCP-tagged and WT RS complex (Oda et al., 2014) enabled us to designate another protrusion as RSP6, which is a paralog of RSP4 in *C. reinhardtii* (Fig. S1). The expected volume of this protrusion (65 $nm^3$) is consistent with that of monomeric RSP6 (56 $nm^3$) (Table 1). In addition, the RSP4 protrusion and RSP6 protrusion bear resemblance morphologically (Fig. 3B), as expected given the sequence similarity and identity between the two proteins.

### Further RS protein assignment by analytical ultracentrifugation and multi-angle light-scattering analysis

To further locate and characterize the other RS head (RSP4, -9 and -10) and neck (RSP16) proteins, we employed analytical ultracentrifugation and multi-angle light-scattering measurements. We expressed RSP4, -9, -10 and -16 using an *E. coli* expression system. Sedimentation velocity and multi-angle light-scattering of each protein indicated that RSP10 dimerizes in solution, whereas RSP4 and RSP9 exist as monomers (Fig. 4), which is in a good agreement with expected volumes from segmentation of our map (Table S1; Fig. 5).

The rest of the volume in one twofold symmetric unit corresponds to two copies of RSP1. Therefore, we assigned RSP1 (dimer), RSP4 (monomer), RSP6 (monomer), RSP9 (monomer) and RSP10 (dimer) in the twofold symmetric unit of the RS head region (Fig. 5A, Table 1). The exact localization of those proteins is based on this and previous biochemical and biophysical studies (see Fig. 5B).

We also attempted to detect interaction between RSP9, -10, and -16 by analytical ultracentrifugation. Previously it was proved that RSP16 forms a dimer (Zhu et al., 2019). However, no pair of these proteins (RSP9–RSP10; RSP9–RSP16 and RSP9–RSP10–RSP16) showed co-sedimentation within the given concentration range *in vitro* (Fig. 4A,B).

**Table 1. Molecular masses of radial spoke proteins of the head and neck regions, their estimated volumes, number of copies, and estimated volumes of RS head and neck regions [based on theory, 2D-nonequilibrium pH gel electrophoresis (2D-NEPHGE; Yang et al. 2006) or the cryo-EM map from this study (SPA)]**

| Radial spoke proteins | Molecular weight (theoretical/2D-NEPHGE) (kDa) | Number of copies | Volume (theoretical/2D-NEPHGE/SPA) ($nm^3$) | Surface model |
|---|---|---|---|---|
| RSP1 | 78.6/123 | 4 | $7.716\times10^5/10.75\times10^5/7.89\times10^5$ |  |
| RSP4 | 49.8/76 | 2 | | |
| RSP6 | 48.8/67 | 2 | | |
| RSP9 | 29.5/26 | 2 | | |
| RSP10 | 23.5/24 | 4 | | |
| RSP2 | 77.4/118 | 4 | $8.23\times10^5/11.79\times10^5/7.51\times10^5$ |  |
| RSP23 | 61/102 | 4 | | |
| RSP16 | 39/34 | 4 | | |

Journal of Cell Science (2020) 133, jcs245233. doi:10.1242/jcs.245233

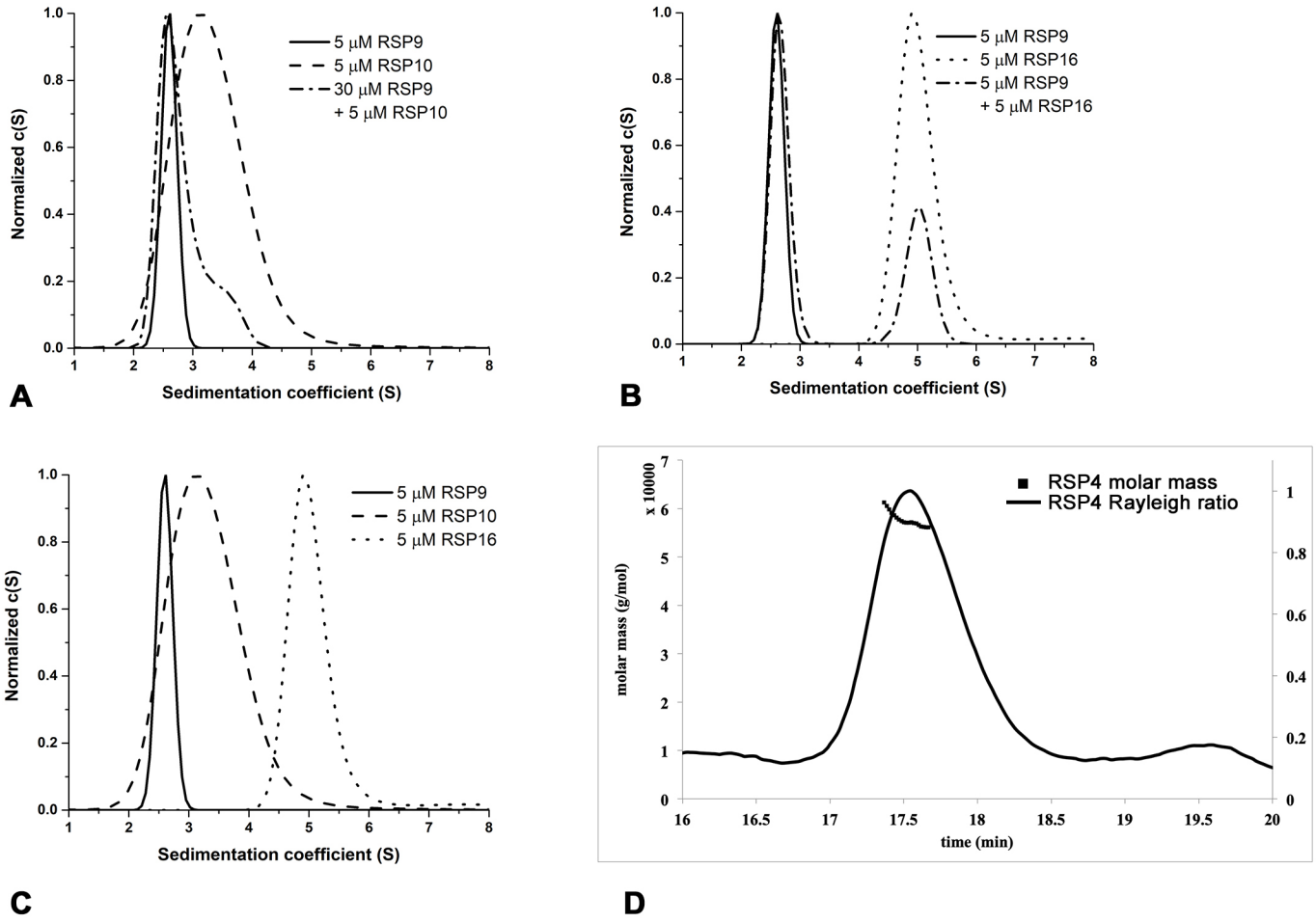


**Fig. 4. Biophysical characterization of the oligomeric state of RSP proteins and their interaction.** RSP proteins were analyzed using sedimentation velocity analytical ultracentrifugation (A–C) and multi-angle light scattering (D).

## DISCUSSION

### Protein organization of the RS head and neck regions

We developed an optimized RS purification procedure by affinity chromatography (Fig. 1) and obtained RS complexes with high purity and yield suitable for electron microscopy studies. Our cryo-electron tomography structure of the 96-nm repeating unit together with the structure of the isolated RS complex using single particle cryo-electron microscopy confirms the presence of twofold symmetry at the RS head region. The stalk region is asymmetric. Therefore, there is a symmetry mismatch in the whole complex, and the junction is at the neck. The refined 15 Å (1.5 nm) resolution reconstruction of the head region represents the most detailed structure observed to date. By combining the structural results with results from cross-linking mass spectrometry, we were able to localize and orient RSP2 and RSP4 in the overall structure. It was the only cross-link between different RS complex proteins, probably due to the small amount of starting material and a significant level of tubulin contamination, which also reacts with DSS. Even though the duplicated spoke proteins have similar domain structures, they have different roles in assembly of the spoke. Both RSP2 and RSP4 are evolutionarily conserved and ubiquitously expressed in ciliated cells, whereas their respective counterparts, RSP23 (also known as NDK5) and RSP6, are not (Zhu et al., 2017a). In line with this, RSP2 and RSP4 are more critical for spoke assembly than RSP23 and RSP6 (Huang et al., 1981; Wei et al., 2010; Zhu et al., 2017a). Our assignment of RSP4 is consistent with a previously reported study on genetically tagged RSP4 (Oda et al., 2014). Their structural map of RSP6-tagged RS complexes enabled us to identify one domain in our structure as RSP6 (gray in Fig. 5). However, their assigned position based on the same map is different from ours. This discrepancy might have occurred because the density assigned as RSP6 in our map was not visible in their reconstruction by cryo-electron tomography. The volumes assigned to RSP4 and RSP6 correspond to the molecular weight of monomers within one twofold symmetric unit.

Currently there is no high-resolution structural data available for any spoke protein to fit into our structure. To further assign RSP components to our density map of the RS head region, we segmented our map (see Materials and Methods) and attempted to assign RSPs based on their volumes and interfaces. The twofold symmetric unit is segmented into six pieces (Fig. 5). Three of them were already assigned as RSP2, -4 and -6. According to previous studies using chemical cross-linking and pull-down assays (Kohno et al., 2011), interfaces should exist between RSP1 and RSP4, RSP4 and RSP9, RSP4 and RSP10, RSP6 and RSP10, RSP6 and RSP9, RSP2 and RSP4, RSP2 and RSP10, as well as RSP1 and RSP23 (Fig. 5B). Assuming that each segmented volume corresponds to an individual RS component, the only possible assignment is as shown in Fig. 5. This segmentation and assignment suggest that RSP10 exists as a dimer, which is supported by our AUC experiment (Fig. 4), whereas RSP1 and RSP9 are dimeric and monomeric,

Journal of Cell Science (2020) 133, jcs245233. doi:10.1242/jcs.245233

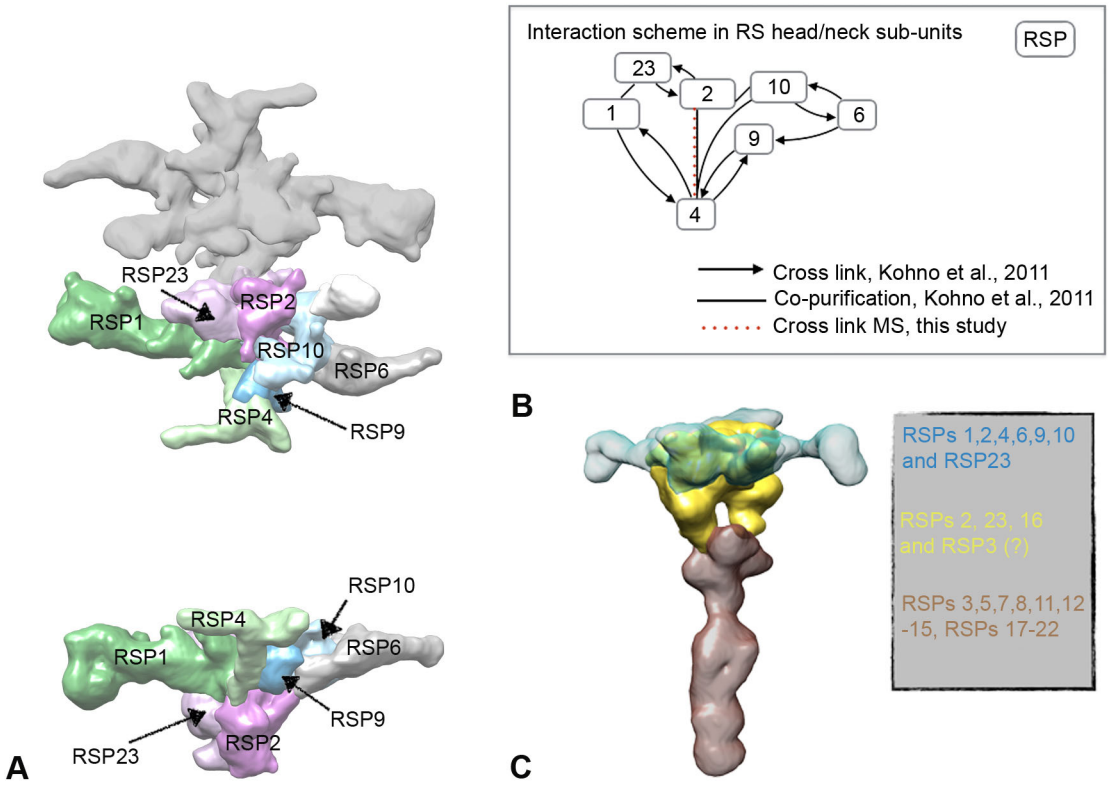


**Fig. 5. Protein organization in the RS complex.** (A) Model of organization in the head and neck region of the RS complex with the following segmentation colors: RSP1 dimer, light green; RSP4 monomer, green; RSP9 monomer, dark blue; RSP10 dimer, light blue; RSP6 monomer, gray; RSP23 dimer, magenta; and RSP2 dimer, violet. (B) Our model, supported by the indicated interactions and cross-link data, suggests two neck proteins – RSP2 and RSP23 – form a part of the spoke head volume and thus the boundaries of the head, neck and stalk regions are redefined. (C) 3D surface-rendered volume of RS complex with redefined boundaries of the head (blue), neck (yellow) and stalk (brown) regions, with corresponding protein composition indicated in the panel.

respectively. We cannot exclude the possibility that the density assigned to RSP1 consists of monomeric RSP1 and the C-terminal region of either RSP2 or RSP3, a model that would be consistent with the suggestion that RSP2 and RSP3 protrude over the radial spoke head (Zhu et al., 2019), as well as with localization of the C terminus of RSP3 being at the level of the spoke head plane (Oda et al., 2014).

In spite of the absence of stable associations between RSP9 and RSP10 in co-sedimentation experiments, we suggest they share a common interaction surface within the head unit stabilized by the interactions between neighboring proteins (Fig. 5). In addition, assignment of RSP9 and RSP10 in the respective segments is consistent with the fact that, although both proteins appeared similar in size and abundance (Piperno et al., 1981), RSP9 is assigned to the segment near the head–neck core, because of its requirements for spoke head assembly (Huang et al., 1981), and is present in the sub-particle containing RSP4, RSP6 and RSP1 (Kohno et al., 2011).

Interestingly the RS neck density extends continuously over the RS head proteins toward the central pair (yellow in Fig. 5B). We therefore suggest that two of the spoke neck proteins, RSP2 and RSP23 partially form the head region of the complex (Fig. 5A, violet and magenta). This also explains an observation from flagella of *ndk5* and *pf24* mutant strains of *C. reinhardtii*, where absence of RSP23 (NDK5) and RSP2, respectively, resulted in absence of spoke head formation despite apparent expression of the corresponding head proteins (Zhu et al., 2017b; Pigino et al., 2011). An absence of co-sedimentation of RSP9 and RSP10 with RSP16 confirms the previously suggested model of RSP16 being localized at the interface between the neck and stalk regions, rather than in the middle of the neck. Thus we have not included the protein in our model of protein organization in the RS head unit.

The current model of spoke protein arrangement suggests the simplest explanation and interpretation of summarized data from this and previous studies on the radial spoke proteins of *C. reinhardtii*. Based on it, we have redefined the boundaries of spoke head, neck and stalk regions (Fig. 5C), where the spoke head (blue) and neck (yellow) have twofold symmetry. The symmetry is broken at the stalk region of the complex (brown). Though there are no *in vitro* data available to define the oligomeric state of RSP2 and RSP23, based on domain prediction of RSP2 and RSP23 (predicted to contain a DPY30 dimerization and docking domain), we propose that both proteins form dimers, suggesting that each bifurcated neck region has one copy of dimeric RSP2, RSP23 and RSP16, respectively. Thus, the total volume of the spoke head and neck regions correlates very well with the theoretical estimation of the total volume of RSPs considering their oligomerization (see Table 1). In order to fully prove the suggested model, one would need to obtain a high-resolution structure of the spoke head region, combined with model building.

Despite the fact that the C terminus of RSP3 was previously shown to protrude towards the bifurcated neck of the spoke complex (Oda et al., 2014) as well as to interact with RSP4 in the pull-down assays by Kohno et al. (2011), C-terminal extension of RSP3 in *Chlamydomonas* is not required for the assembly of the spoke head (Sivadas et al., 2012). Thus, there is insufficient evidence of its localization at the head region of the complex to assign that region of RSP3 to our symmetrized map

Journal of Cell Science (2020) 133, jcs245233. doi:10.1242/jcs.245233

### Comparison of protein organization of the RS head in *C. reinhardtii* and mammals

Previously reported studies suggest that genetic mutations in three of the human spoke head proteins, RSPH1, RSPH9 and RSPH4a are involved in primary ciliary diskynesia (Castelman et al., 2009; Knowles et al., 2014). The overall structure of the RS1 and RS2 head region in humans (Lin et al., 2014) and *Chlamydomonas* (current work) looks slightly different. In both organisms the head region has a twofold symmetry. However, the RS head in *Chlamydomonas* has rather a large area that faces the central pairs, whereas in humans there are two narrow parallel densities protruding laterally from the center of symmetry. RSP1 of *C. reinhardtii* is evidently longer (814 amino acids) compared with the human ortholog RSPH1 (only 309 amino acids, accession number: AAI01520) and thus might occupy a bigger volume in the head structure. Thus the molecular interactions can substantially change along with the sequence differences in the RS head proteins of different species.

### Pseudo-twofold symmetry of the RS complex in beating of flagella

Structural and functional studies of *Chlamydomonas* cilia with genetic tagging and truncation of RS and central pair (CP) proteins strongly suggest that one of the main roles of the RS head region is in rather mechanical, transient interactions with the central pair, or more precisely its projections C1a and C1b, in the process of flagella beating (Oda et al., 2014). Considering the periodicity of projections along the CP apparatus and the 32-nm distances between RS1 and RS2 (Pigino et al., 2011), it is not surprising to see the head regions of RS1 and RS2 being structurally identical. Thus, the spoke complex consists of a symmetric head, which is most probably a mechanical sensor. After interaction between the CP projections and the twofold symmetric RS head, the signal is transduced to the asymmetric neck/stalk unit, regulated biochemically (for example, by calcium release or phosphorylation; see Smith and Yang, 2004) and finally transferred further down to the inner dynein arms and microtubule doublets.

## MATERIALS AND METHODS

### Cell culture and sample preparation

The wild-type strain of *C. reinhardtii* used for cryo-electron tomography studies (137c) was obtained from the Chlamydomonas Resource Center (University of Minnesota, St Paul, MN). The mutant strain used for conventional (*pf28pf30*) isolation of the spoke complex was kindly obtained from Professor David Mitchel (NYU, Stoney Brook, New York). The strain used for optimized isolation of the complex (full-length: a strain expressing 12×His-tagged RSP3) is based on the construct designed in our previous work (Sivadas et al., 2012). The cells were cultured in TAP (Tris-acetate-phosphate) medium (Gorman and Levine, 1965).

### Flagella isolation for cryo-electron tomography

Flagella were isolated from *Chlamydomonas* cells based on the protocol of Witman (1986), with modification. After growing to steady state, cells were harvested at 1000 ***g*** and flagella were amputated using dibucaine. Flagella were sedimented at 12,000 ***g*** for 20 min at 4°C, de-membraned with 1% IGEPAL (CA-630, Merck) in a buffer containing 20 mM HEPES (pH 7.5), 5 mM $MgSO_4$, 1 mM dithiothreitol (DTT), 0.5 mM EDTA, and 25 mM KCl before being sedimented again at 12,000 ***g*** for 2 min at 4°C. The pellet of axonemes was resuspended in the same buffer, and adjusted to an appropriate concentration followed by plunge freezing in liquid ethane.

### Radial spoke purification

#### Sucrose density gradient-based purification

6×4 L of densely cultured *C. reinhardtii* cells from either WT or *pf28 pf30* mutant strains were harvested at 1200 ***g*** for 6 min at 20°C and resuspended in 150 ml of 10 mM HEPES buffer, pH 7.5. Deflagellation was carried out using the pH shock method (Craige et al., 2013) with a buffer consisting of 10 mM HEPES (pH 7.5), 4% sucrose, 5 mM $MgSO_4$, 0.5 mM EGTA and protease inhibitor cocktail (Roche cOmplete). To separate cell bodies from flagella, sedimentation was carried out using a 30% sucrose cushion at 2000 ***g*** for 10 min at 4°C, with minimal acceleration and deceleration. Sedimentation was repeated without the sucrose cushion at 3200 ***g*** for 5 min at 4°C. The flagella pellet was further clarified by sedimentation at 12,000 ***g*** for 20 min at 4°C and then resuspended into a buffer consisting of 10 mM HEPES, pH 7.5, 5 mM $MgSO_4$, 1 mM β-mercaptoethanol (BME), 0.5 mM EDTA, 25 mM KCL and EDTA-free protease inhibitor cocktail (Roche cOmplete). At this step, typical flagella concentration was in the range of 4–8 mg/ml. Demembranation of flagella was performed using 1% IGEPAL with two incubations for 10 min at 4°C. The efficacy of demembranation was examined under a phase-contrast microscope. Thereafter isolated axonemes were treated twice with 0.5 M KCl or NaCl to remove dyneins, then sedimented at 13,000 ***g*** for 1–2 min at 4°C. For extraction of the spoke complex, the pellet of typically 6–8 mg/ml (calculated from absorbance at 280 nm) was incubated with 0.6 M KI for 15 min at 4°C following a 1:1 dilution with 10 mM HEPES pH 7.5, 5 mM $MgSO_4$, 1 mM BME, 0.5 mM EDTA, 25 mM KCl and protease inhibitor cocktail (Roche cOmplete, EDTA-free). The clarified pellet with the RS complex was carefully layered on top of a 10–30% linear sucrose gradient (3 ml volume) containing 0.4 M NaCl in the buffer. After ∼12–13 h ultracentrifugation using a Beckman SW41 Ti rotor at 32,000× rpm (∼175,000 ***g***), 20 fractions were manually collected in a top to bottom manner.

#### Optimized purification procedure

2×4 L of *C. reinhardtii* cells from transgenic 12×His-tagged *full-length* strain were used to isolate RS complexes as described above. Following further purification of the RS fraction from tubulin aggregates by sedimentation at 16,000 ***g*** for 20 min at 4°C, the supernatant was loaded onto 200–500 µl $Co^{2+}$ TALON beads slurry (MERCK, previously Sigma Aldrich) and, after several washes with 0.5 M NaCl, elution was carried out using a buffer (10 mM HEPES, 5 mM $MgSO_4$, EGTA-free protease inhibitor cocktail, 25 mM KCl, and 1 mM BME) containing 0.5 M imidazole.

### EM grid preparation

For negative stain TEM, 3.5–4 µl of purified RS complex was first applied to a carbon grid (Plano, Germany), thereafter excess liquid was blotted away with the help of filter paper and the grid was stained with 1–2% uranyl acetate solution.

For cryo-electron tomography, we mounted 3.5 µl solution of flagella on a Quantifoil R3.5/1 grid and used a one-side blotting and plunging method using the Gatan CP-3, as described in Bui and Ishikawa (2013).

For cryo-grid preparation for single particle analysis, following the affinity purification, 3.5 µl of purified RS complex was applied to holey grids with a continuous carbon layer (Quantifoil R2/1, 200 mesh size). Excess liquid was blotted from the back, and the grid was rapidly plunge frozen in liquid ethane with either a manual plunge freezing device or double-side blotted with a Vitrobot Mark III (Thermo Fisher, USA).

### Cryo-EM data collection

The cryo-electron tomography datasets were acquired by a Titan Krios TEM with GIF Quantum and a K2 detector (Gatan, AMETEK) using SerialEM software (Mastronarde, 2005) with dose fractionation (7–10 frames/micrograph) and a total dose of ∼60 e/Å$^2$, following the protocol of Bui and Ishikawa (2013). Single particle cryo-EM data were collected using a Falcon 2 direct detector and Tecnai/F20 electron microscope (FEI, currently ThermoFisher) with 18–20 e/Å$^2$ dose and acquisition of 7 frames/s using EPU (FEI).

### Image analysis

Tomograms were reconstructed using IMOD (Mastronarde and Held, 2017). Sub-tomograms were aligned and averaged as described previously (Bui and Ishikawa, 2013).

Journal of Cell Science (2020) 133, jcs245233. doi:10.1242/jcs.245233

Single particle cryo-EM data were analyzed using RELION2.1 software (Scheres, 2012). First, movies were drift corrected using MOTIONCORR software (Li et al., 2013) and CTF was corrected using CTFFIND4 (Rohou and Grigorieff, 2015). After that, particles were picked using semi-automatic picking procedures, resulting in total of ∼240 kX particles. This was followed by 2D classification procedures. Thereafter 3D classification was performed, using a ∼40 Å (4 nm) RS structure from cryo-electron tomography as an initial reference (EMD-1941; Pigino et al., 2011). In the second stage, we masked the radial spoke heads as well as part of the neck region and analyzed, assuming twofold symmetry.

We defined the correct contour level for the sub-tomogram average, based on the theoretical volume of one tubulin dimer, assuming 1.21 $Å^3$/Da conversion (Harpaz et al., 1994). After that we adjusted the contour level of unsymmetrized/symmetrized RS structures from single particle analysis to fit the volume of RS1 from 96 nm sub-tomogram average. Then we segmented the map from single particle analysis using the Segger package (Pintilie et al., 2010) from the UCSF Chimera software (Pettersen et al., 2004) with smoothing step 5, step size of 1 voxel and surface granularity of 1 voxel, combining with the manual grouping of the regions resulting in 11 segments within one symmetric unit. We started by grouping the segments corresponding to the position and volumes of monomeric RSP4, dimeric RSP2 and monomeric RSP6. The segmented volumes between RSP4 and RSP6 were grouped to assign corresponding volumes of monomeric RSP9 and dimeric RSP10. The rest of the segments were assigned to corresponding dimers of RSP1 and RSP23.

Mass calculations of the head, neck and stalk regions of the RS complex were performed using the average protein density of 1.43 $g/cm^3$, as described in Quillin and Matthews (2000).

## Biochemical analysis

### Protein expression and purification

Recombinant RSP4, -9, -10 and -16 were produced by *E. coli*, carrying corresponding coding sequences in the pProEx (RSP16), Egwomipi (plasmid kindly provided by Dr Rolf Jaussi, Paul Scherrer Institut, Switzerland) (RSP4) and PSTCm1 (kindly obtained from Dr N. Olieric, Paul Scherrer Institut, Switzerland) (RSP9 and RSP10) plasmids. Expression was induced using 1 mM isopropyl-β-d-thiogalactopyranosid for 12 h at 20°C. Cells suspended with 500 mM NaCl, 10 mM imidazole, 5 mM β-mercapthoethanol, and protease inhibitor cocktail (cOmplete, EDTA-free, Roche) in 50 mM HEPES (pH 7.5) were lysed by sonication. Following centrifugation at 30,000 rpm (∼104,350 ***g***) with a Ti45 rotor (Beckman Coulter, Indianapolis, IN) for 30 min at 4°C, His–RSPs in supernatant filtered through 0.45-µm filter membranes were purified by IMAC $Ni^{2+}$ affinity chromatography using an AKTA express system, following the instructions of the manufacturer (GE Healthcare Life Science, Wauwatosa, WI). The eluate was concentrated.

### Analytical ultracentrifugation and multi-angle light scattering

Sedimentation velocity experiments were performed at 20°C and 42,000 rpm (∼147,000 ***g***) in a Beckman Coulter ProteomeLab XL-I analytical ultracentrifuge using standard protocols (Zhao et al., 2013; Brown et al., 2008). Sedimentation data were collected with absorbance optical systems and analyzed in terms of a continuous c(s) distribution of Lamm equation solutions with the software SEDFIT (Schuck et al., 2000; Rezabkova et al., 2016).

A multi-angle light-scattering device from Wyatt Technology miniDAWN TREOS and Wyatt Optilab T-rEX RI detector coupled to a size exclusion chromatography column was used to determine oligomeric states of RSP4,9 and -10 *in vitro*. Measurements were performed using a UV-VIS diode system set to 280 nm wavelength, and a MALS detector wavelength of 658 nm and RI detector wavelength of 660 nm. Buffers were filtered with 0.45-um filters prior running through the system for aggregation removal. The column was equilibrated in 20 mM Tris (pH 7.5), 150 mM NaCl, 2 mM DTT buffer, after which 120 µl of protein were injected at concentrations between 0.6–3 mg/ml with a flow rate of 0.4–0.5 ml/min and temperature of 25°C.

Prior to performing binding experiments, proteins were premixed in a 1:1 ratio at 1–3 mg/ml concentrations and either incubated at 4°C for 1 h or directly injected onto the column.

### Cross-linking mass spectrometry

400 µl (settled) TALON beads containing approximately 25 µg of bound RSP preparation were first washed with cross-linking buffer (10 mM HEPES pH 7.4, 1 mM β-mercaptoethanol, 5 mM $MgSO_4$, 0.5 mM EGTA) plus 500 mM KCl, and then with cross-linking buffer alone. Beads were resuspended in 400 µl cross-linking buffer and split into two aliquots. One aliquot was incubated with 500 µM DSS (DSS-$d_0$/$d_{12}$; Creative Molecules), the other with 125 µM DSS. The cross-linking reaction was allowed to proceed for 50 min at 25°C with mild shaking, then quenched by addition of ammonium bicarbonate to 50 mM final concentration and further incubation for 30 min.

Cross-linked proteins were subjected to reduction with Tris(2-carboxyethyl)phosphine, alkylation with iodoacetamide and proteolysis with endoproteinase Lys-C (Wako; 3 h at 37°C) and trypsin (Promega; overnight at 37°C) according to standard procedures. The supernatant was removed and purified by solid-phase extraction (SepPak tC18 cartridges; Waters) prior to size-exclusion fractionation (Superdex Peptide PC 3.2/300; GE), as previously described (Leitner et al., 2012). Three fractions were collected and analyzed by liquid chromatography–tandem mass spectrometry on an Orbitrap Fusion Lumos mass spectrometer (Thermo Fisher Scientific), as described previously (Wongpalee et al., 2019).

Mass spectrometry data were searched using xQuest (Leitner et al., 2014) against a database containing the sequences of 17 radial spoke proteins together with 21 associated proteins and contaminants (including tubulin, dynein and human keratins) and the corresponding decoy database containing shuffled sequences. Specific search settings were as follows: enzyme=trypsin, maximum number of missed cleavages=2, mass tolerance for initial search=15 p.p.m. for MS data and 0.2/0.3 Da for MS/MS data. Search results were further filtered according to the actual MS1 error of ±3 p.p.m., a %TIC sub-score of ≥0.1 and a delta score of ≤0.9. All remaining spectra were manually evaluated and candidate cross-link identifications were only retained if spectra contained at least four bond cleavages overall or three consecutive ones per peptide. The selected xQuest score thresholds of 19 for intra-protein and 26 for inter-protein cross-links did not result in any decoy hits. All identified cross-linked peptides are listed in Table S2. Mass spectrometry data have been deposited at the ProteomeXchange Consortium via the PRIDE partner repository (Perez-Riverol et al., 2019) with the dataset identifier PXD015658.

#### Acknowledgements

We are grateful to ScopeM at ETH Zurich and the EM facility at the Paul Scherrer Institute for technical support on electron microscopy.

#### Competing interests

The authors declare no competing or financial interests.

#### Author contributions

Conceptualization: T.I., E.P.; Methodology: E.P., P.Y., D.R.D., T.I.; Validation: E.P., A.L., L.F., T.I.; Formal analysis: E.P., L.F., I.I., A.L., T.I.; Investigation: E.P., I.I., L.F., A.L., T.I.; Resources: E.P., I.I., B.Z., A.L., R.A., T.I., P.Y.; Writing - original draft: E.P., L.F., A.L., P.Y., D.R.D., T.I.; Writing - review & editing: E.P., I.I., A.L., P.Y., D.R.D., R.A., B.Z., T.I.; Visualization: E.P., L.F.; Supervision: D.R.D., T.I.; Project administration: T.I.; Funding acquisition: R.A., T.I.

#### Funding

This project was funded by grants from the Schweizerischer Nationalfonds zur Förderung der Wissenschaftlichen Forschung to T.I. (NF31003A_166617 and NF31003A_144035). Cross-linking mass spectrometry experiments were supported by a grant from the European Research Council (ERC AdG 679821) to R.A.

#### Data availability

Cryo-EM density maps are deposited in the EM Databank (EMD-11085 and EMD-11086). Mass spectrometry data have been deposited at the ProteomeXchange Consortium via the PRIDE partner repository with the dataset identifier PXD015658.

#### Supplementary information

Supplementary information available online at
https://jcs.biologists.org/lookup/doi/10.1242/jcs.245233.supplemental

**Peer review history**
The peer review history is available online at
https://jcs.biologists.org/lookup/doi/10.1242/jcs.245233.reviewer-comments.pdf

**References**

**Barber, C. F., Heuser, T., Carbajal-Gonzalez, B. I., Botchkarev, V. V., Jr and Nicastro, D.**, (2012). Three-dimensional structure of the radial spokes reveals heterogeneity and interactions with dyneins in Chlamydomonas flagella. *Mol. Biol. Cell* **23**, 111-120. doi:10.1091/mbc.e11-08-0692

**Brown, P. H., Balbo, A. and Schuck, P.**, (2008). Characterizing protein-protein interactions by sedimentation velocity analytical ultracentrifugation. *Curr. Protoc. Immunol.* **81**, 18.15.1-18.15.39. doi:10.1002/0471142735.im1815s81

**Bui, K. H. and Ishikawa, T.** (2013). 3D structural analysis of flagella/cilia by cryo-electron tomography. *Methods Enzymol.* **524**, 305-323. doi:10.1016/B978-0-12-397945-2.00017-2

**Castelman, V. H., Romio, L., Chodhari, R., Hirst, R. A., de Castro, S. C. P., Parker, K. A., Ybot-Gonzalez, P., Emes, R. D., Wilson, S. W., Wallis, C. et al.** (2009). Mutations in radial spoke head protein genes RSPH9 and RSPH4A cause primary ciliary dyskinesia with central-microtubular-pair abnormalities. *Am. J. Hum. Genet.* **84**, 197-209. doi:10.1016/j.ajhg.2009.01.011

**Craige B., Brown J. M. and Witman G. B.** (2013). Isolation of Chlamydomonas Flagella. *Curr. Protoc. Cell Biol.* **59**, 3.41.1-3.41.9. doi:10.1002/0471143030.cb0341s59

**Gorman D. S. and Levine R. P.** (1965). Cytochrome f and plastocyanin: their sequence in the photosynthetic electron transport chain of Chlamydomonas reinhardti. *Proc. Natl. Acad. Sci. USA* **54**, 1665-1669. doi:10.1073/pnas.54.6.1665

**Harpaz, Y., Gerstein, M. and Chothia, C.** (1994). Volume changes on protein folding. *Structure* **2**, 641-649. doi:10.1016/s0969-2126(00)00065-4

**Herzog, F., Kahraman, A., Boehringer, D., Mak, R., Bracher, A., Walzthoeni, T., Leitner, A., Beck, M., Harti, F.-U., Ban, N. et al.** (2012). Structural probing of a protein phosphatase 2A network by chemical cross-linking and mass spectrometry. *Science* **337**, 1348-1352. doi:10.1126/science.1221483

**Huang, B., Piperno, G., Ramanis, Z. and Luck, D. J.** (1981). Radial spokes of Chlamydomonas flagella: genetic analysis of assembly and function. *J. Cell Biol.* **88**, 80-88. doi:10.1083/jcb.88.1.80

**Kelekar, P., Wei, M. and Yang, P.** (2009). Isolation and analysis of radial spoke proteins. *Methods Cell Biol.* **92**, 181-196. doi:10.1016/S0091-679X(08)92012-4

**Knowles, M. R., Ostrowski, L. E., Leigh, M. W., Sears, P. R., Davis, S. D., Wolf, W. E., Hazucha, M. J., Carson, K. L., Olivier, K. N., Sagel, S. D. et al.** (2014). Mutations in RSPH1 cause primary ciliary dyskinesia with a unique clinical and ciliary phenotype. *Am. J. Respir. Crit. Care Med.* **189**, 707-717. doi:10.1164/rccm.201311-2047OC

**Kohno, T., Wakabayashi, K.-I., Diener, D. R., Rosenbaum, J. L. and Kamiya, R.** (2011). Subunit interactions within the Chlamydomonas flagellar spokehead. *Cytoskeleton (Hoboken)* **68**, 237-246. doi:10.1002/cm.20507

**Leitner, A., Reischi, R., Walzthoeni, T., Herzog, F., Bohn, S., Förster, F. and Aebersold, R.** (2012). Expanding the chemical cross-linking toolbox by the use of multiple proteases and enrichment by size exclusion chromatography. *Mol. Cell Proteomics* **11**, M111.014126. doi:10.1074/mcp.M111.014126

**Leitner, A., Walzthoeni, T. and Aebersold, R.** (2014). Lysine-specific chemical cross-linking of protein complexes and identification of cross-linking sites using LC-MS/MS and the xQuest/xProphet software pipeline. *Nat. Protoc.* **9**, 120-137. doi:10.1038/nprot.2013.168

**Leitner, A., Faini, M., Stengel, F. and Aebersold, R.** (2016). Crosslinking and mass spectrometry: an integrated technology to understand the structure and function of molecular machines. *Trends Biochem. Sci.* **41**, 20-32. doi:10.1016/j.tibs.2015.10.008

**Li, X., Mooney, P., Zheng, S., Booth, C. R., Braungeld, M. B., Gubbens, S., Agard, D. A. and Cheng, Y.** (2013). Electron counting and beam-induced motion correction enable near-atomic resolution single-particle cryo-EM. *Nat. Methods* **10**, 584-590. doi:10.1038/nmeth.2472

**Lin, J., Yin, W., Smith, M. C., Song, K., Leigh, M. W., Zariwala, M. A., Knowles, M. R., Ostrowski, L. E. and Nicastro, D.** (2014). Cryo-electron tomography reveals ciliary defects underlying human RSPH1 primary ciliary dyskinesia. *Nat. Commun.* **5**, 5727. doi:10.1038/ncomms6727

**Mastronarde, D. N.** (2005). Automated electron microscope tomography using robust prediction of specimen movements. *J. Struct. Biol.* **152**, 26-51. doi:10.1016/j.jsb.2005.07.007

**Mastronarde, D. N. and Held, S. R.** (2017). Automated tilt series alignment and tomographic reconstruction in IMOD. *J. Struct. Biol.* **197**, 102-113. doi:10.1016/j.jsb.2016.07.011

**Oda, T., Yanagisawa, H., Yagi, T. and Kikkawa, M.** (2014). Mechanosignaling between central apparatus and radial spokes controls axonemal dynein activity. *J. Cell Biol.* **204**, 807-819. doi:10.1083/jcb.201312014

**Patel-King, R. S., Gorbatyuk, O., Takebe, S. and King, S. M.** (2004). Flagellar radial spokes contain a Ca2+ -stimulated nucleoside diphosphate kinase. *Mol. Biol. Cell* **15**, 3891-3902. doi:10.1091/mbc.e04-04-0352

**Perez-Riverol, Y., Csordas, A., Bai, J., Bernal-Llinares, M., Hewapathirana, S., Kundu, D. J., Inuganti, A., Griss, J., Mayer, G., Eisenacher, M. et al.** (2019). The PRIDE database and related tools and resources in 2019: improving support for quantification data. *Nucleic Acids Res.* **47**, D442-D450. doi:10.1093/nar/gky1106

**Pettersen, E. F., Goddard, T. D., Huang, C. C., Couch, G. S., Greenblatt, D. M., Meng, E. C. and Ferrin, T. E.** (2004). UCSF Chimera—a visualization system for exploratory research and analysis. *J. Comput. Chem.* **25**, 1605-1612. doi:10.1002/jcc.20084

**Pigino, G., Bui, K. H., Maheshwari, A., Lupetti, P., Diener, D. and Ishikawa, T.** (2011). Cryoelectron tomography of radial spokes in cilia and flagella. *J. Cell Biol.* **195**, 673-687. doi:10.1083/jcb.201106125

**Pigino, G., Maheshwari, A., Bui, K. H., Shingyoji, C., Kamimura, S. and Ishikawa, T.** (2012). Comparative structural analysis of eukaryotic flagella and cilia from Chlamydomonas, Tetrahymena, and sea urchins. *J. Struct. Biol.* **178**, 199-206. doi:10.1016/j.jsb.2012.02.012

**Pintilie, G. D., Zhang, J., Goddard, T. D., Chiu, W. and Gossard, D. C.** (2010). Quantitative analysis of cryo-EM density map segmentation by watershed and scale-space filtering, and fitting of structures by alignment to regions. *J. Struct. Biol.* **170**, 427-438. doi:10.1016/j.jsb.2010.03.007

**Piperno, G., Huang, B., Ramanis, Z. and Luck, D. J.** (1981). Radial Spokes of Chlamydomonas flagella: polypeptide composition and phosphorylation of stalk components. *J. Cell Biol.* **88**, 73-79. doi:10.1083/jcb.88.1.73

**Quillin, M. L. and Matthews, B. W.** (2000). Accurate calculation of the density of proteins. *Acta Crystallogr. D Biol. Crystallogr.* **56**, 791-794. doi:10.1107/S090744490000679X

**Rezabkova, L., Kraatz, S. HW., Akhmanova, A., Steinmetz, M. O. and Kammerer, R. A.** (2016). Biophysical and structural characterization of the centriolar protein Cep104 interaction network. *J. Biol. Chem.* **291**, 18496-18504. doi:10.1074/jbc.M116.739771

**Rohou, A. and Grigorieff, N.** (2015). CTFFIND4: fast and accurate defocus estimation from electron micrographs. *J. Struct. Biol.* **192**, 216-221. doi:10.1016/j.jsb.2015.08.008

**Scheres, S. HW.** (2012). RELION: implementation of a Bayesian approach to cryo-EM structure determination. *J. Struct Biol.* **180**, 519-530. doi:10.1016/j.jsb.2012.09.006

**Schuck, P.** (2000). Size-distribution analysis of macromolecules by sedimentation velocity ultracentrifugation and lamm equation modeling. *Biophys. J.* **78**, 1606-1619. doi:10.1016/s0006-3495(00)76713-0

**Sivadas, P., Dienes, J. M., St. Maurice, M., Meek, W. D. and Yang, P.** (2012). A flagellar A-kinase anchoring protein with two amphipathic helices forms a structural scaffold in the radial spoke complex. *J. Cell Biol.* **199**:639-651. doi:10.1083/jcb.201111042

**Smith, E. F. and Yang, P.** (2004). The radial spokes and central apparatus: mechano-chemical transducers that regulate flagellar motility. *Cell Motil. Med.* **300**, 53-56.

**Wei, M., Sivadas, P., Owen, H. A., Mitchell, D. R. and Yang, P.** (2010). Chlamydomonas mutants display reversible deficiencies in flagellar beating and axonemal assembly. *Cytoskeleton (Hoboken)* **67**, 71-80. doi:10.1002/cm.20422

**Witman, G. B.** (1986). Isolation of Chlamydomonas flagella and flagellar axonemes. *Methods Enzymol.* **134**, 280-290. doi:10.1016/0076-6879(86)34096-5

**Wongpalee, S. P., Liu, S., Gallego-Bartolomé, J., Leitner, A., Aebersold, R., Liu, W., Yen, L., Nohales, M. A. Kuo, P. H., Vashisht, A. A. et al.** (2019). CryoEM structures of Arabidopsis DDR complexes involved in RNA-directed DNA methylation. *Nat. Commun.* **10**, 3916. doi:10.1038/s41467-019-11759-9

**Yang, P., Diener, D. R., Rosenbaum, J. L. and Sale, W. S.** (2001). Localization of Calmodulin and Dynein light chain LC8 in flagellar radial spokes. *J. Cell Biol.* **153**, 1315-1326. doi:10.1083/jcb.153.6.1315

**Yang, P., Diener, D. R., Yang, C., Kohno, T., Pazout, G. J., Dienes, J. M., Agrin, N. S., King, S. M., Sale, W. S., Kamiya, R. et al.** (2006). Radial spoke proteins of Chlamydomonas flagella. *J.Cell Sci.* **119**, 1165-1174. doi:10.1242/jcs.02811

**Zhao, H., Brautigam, C. A., Ghirlando, R. and Schuck, P.** (2013). Overview of current methods in sedimentation velocity and sedimentation equilibrium analytical ultracentrifugation. *Curr. Protoc. Protein Sci.* Chapter 20, unit 20.12. doi:10.1002/0471140864.ps2012s71

**Zhu, X., Liu, Y. and Yang, P.** (2017a). Radial Spokes-A snapshot of the motility regulation, assembly, and evolution of cilia and flagella. *Cold Spring Harb. Perspect. Biol.* **9**, a028126. doi:10.1101/cshperspect.a028126

**Zhu, X., Poghosyan, E., Gopal, R., Liu, Y., Ciruelas, K. S., Maizy, Y., Diener, D. R., King, S. M., Ishikawa, T. and Yang, P.** (2017b). General and specific promotion of flagellar assembly by a flagellar nucleoside diphosphate kinase. *Mol. Biol. Cell* **28**, 3029-3042. doi:10.1091/mbc.e17-03-0156

**Zhu, X., Poghosyan, E., Rezabkova, L., Mehall, B., Sakakibara, H., Hirono, M., Kamiya, R., Ishikawa, T. and Yang, P.** (2019). The roles of a flagellar HSP40 ensuring rhythmic beating. *Mol. Biol. Cell* **30**, 228-241. doi:10.1091/mbc.E18-01-0047